Environ Monit Assess (2020) 192: 123
https://doi.org/10.1007/s10661-020-8094-8

Spatiotemporal shoreline dynamics of Marismas Nacionales, Pacific coast of Mexico, based on a remote sensing and GIS mapping approach

Luis Valderrama-Landeros · Manuel Blanco y Correa · Francisco Flores-Verdugo · León Felipe Álvarez-Sánchez · Francisco Flores-de-Santiago

Received: 6 July 2019 / Accepted: 14 January 2020 / Published online: 18 January 2020

Abstract Within the last few decades, tropical coastal systems such as beaches, dunes, and mangrove forests have experienced high annual rates of loss worldwide due to natural and anthropogenic impacts. Historical remote sensing data have been used to map and monitor these fragile systems, as well as to track specific events through time. The purpose of this study was to examine coastal trends along Marismas Nacionales in Mexico, which is the largest wetland complex of the western coast of the Pacific Ocean. The opening of the Cuautla Canal in 1976 and the construction of several hydroelectric power dams have severely impacted this wetland system. Shoreline variability was estimated based on representative remote sensing images over half a century (1970 to 2019). Results indicate that, after 49 years, 805 ha of beach deposits have been lost in the Cuautla Canal and at the beach ridge region that should otherwise be an accretional coastal zone. Conversely, the southern section of the study site shows 406 ha of constant accretion during the same period due to the presence of the unobstructed San Pedro River. Our study highlights the adverse effects of engineering projects, such as inlets and hydroelectric dams throughout tropical coastal systems that have strongly depended on freshwater input from upstream rivers.

Keywords Estuary · Coastal lagoon · Landsat · SPOT · Sentinel

Manuel Blanco Correa is deceased. This paper is dedicated to his memory.

L. Valderrama-Landeros
Subcoordinación de Percepción Remota, Comisión Nacional Para el Conocimiento y Uso de la Biodiversidad (CONABIO), 4903 Liga Periférico-Insurgentes Sur, Tlalpan, 14010 Mexico, City, Mexico

M. Blanco y Correa
Secretaria de Investigación y Posgrado, Universidad Autónoma de Nayarit, Boulevard Tepic-Xalisco 325, Ciudad de la Cultura, 63155 Tepic, Nayarit, Mexico

F. Flores-Verdugo
Instituto de Ciencias del Mar y Limnología. Unidad Académica Mazatlán, Universidad Nacional Autónoma de México, Av. Joel Montes Camarena s/n, 82040 Mazatlán, Sinaloa, Mexico

L. F. Álvarez-Sánchez
Instituto de Ciencias del Mar y Limnología. Unidad de Informática Marina, Universidad Nacional Autónoma de México, CU, Av. Universidad 3000, Coyoacán, 04510 Mexico, City, Mexico

F. Flores-de-Santiago (✉)
Instituto de Ciencias del Mar y Limnología. Unidad Académica Procesos Oceánicos y Costeros, Universidad Nacional Autónoma de México, Av. Universidad 3000 CU, Coyoacán, 04510 Mexico, City, Mexico
e-mail: floresdesantiago@gmail.com

Introduction

Tropical intertidal ecosystems (e.g., tidal marshes, beaches, barrier islands, coral reefs, seagrasses, and mangrove forests) are dynamic environments owing to the presence of abiotic gradients (Rogers et al. 2019), wave exposure (Román-Rivera and Ellis 2019), sediment dynamics (Bishop et al. 2017), and seasonal soil salinity variability (Ouyang et al. 2017). These habitats

likewise serve as critical nesting areas for many wildlife species of high conservation concern (Powell et al. 2019), as well as an essential nursery habitat for commercial fisheries (Mahoney and Bishop 2017). Unfortunately, anthropogenic impacts on coastal ecosystems have been notable over large scales, with habitat loss due to land alterations, such as conversion of wetlands into shrimp farms (Ahmed and Glaser 2016), lack of freshwater availability (Valderrama-Landeros and Flores-de-Santiago 2019), and alteration of coastal hydrology and geomorphology due to the introduction of artificial coastal structures (Perkins et al. 2015). For example, shore-parallel (e.g., seawall and breakwaters) and shore-perpendicular structures (e.g., groins, canals) affect wave rarefaction, littoral currents, and sediment dynamics, and thus biotic responses (Bishop et al. 2017). The magnitude of these impacts varies according to the design, location (i.e., site-specific), and tidal elevation, thus the methods or techniques used to assess ecosystem degradation depend on the study site (Román-Rivera and Ellis 2019). Moreover, the geomorphological effects of these coastal perturbations are likely to be intensified by the impacts of climate change, such as the predicted sea-level rise of 30 to 180 cm by 2100 (McLeman 2018; Powell et al. 2019) and the increasing frequency of tropical storms and hurricanes (Perkins et al. 2015).

Monitoring the spatiotemporal variability of intertidal environments has been an essential ecological aim during the last decades because of the persistent degradation of biogenic habitats worldwide (Mahoney and Bishop 2017). Traditional monitoring assessments are commonly based on historical coastline trends (e.g., Nassar et al. 2018; Williams et al. 2018) and changes in species composition (e.g., Mahoney and Bishop 2017). Concerning the estimation of coastal variability, even though in situ methods, such as topographic surveys, have made the task of repeatedly measuring shoal and beach profiles easier, these methods are still time-consuming, expensive, and spatially limited (Román-Rivera and Ellis 2019). Furthermore, harsh coastal conditions, such as saline environment, water-level changes related to tidal fluctuations, and storm waves, could permanently damage electronic field instrumentation, hindering the feasibility of field-based surveys.

An alternative approach to coping with in situ limitations could be the use of geographic information systems (Harik et al., 2017), multi-criteria decision analysis (Maanan et al., 2018), and remote sensing technologies. For instance, historical remote sensing images could be retrieved from data servers or even from analog air photographs. These remote sensing sensors could cover a considerable area during a single capture, providing a cost-effective option that allows the systematic and repeatedly global study of coastal systems, thus alleviating many of the challenges related to field endeavors (Gens 2010). However, there are still limitations regarding the spatial and temporal capacity of some remote sensing sensors (Román-Rivera and Ellis 2019). For instance, spatial resolution (i.e., pixel size) determines the amount of detail from every image. Also, data acquisition from passive sensors (e.g., Landsat, SPOT, Sentinel, IKONOS, and WorldView) is hampered by cloud cover, which is a common situation along tropical and temperate latitudes. Moreover, the revisiting scene time (i.e., temporal resolution) depends on the satellite orbit and is not possible to modify in most platforms, limiting the number of free-cloud available images for a particular location. Nevertheless, remote sensing technology will continue to advance, increasing the acquisition and processing of spaceborne data, which will eventually allow a more comprehensive and complete framework of coastal geomorphological analyses.

Multiple remote sensing endeavors have been done to study coastal geomorphology trends (see reviews by Gens 2010; Leuven et al. 2016; Román-Rivera and Ellis 2019; Williams et al. 2018). Based on such studies, it is clear that coastline trends are mainly associated with tides, waves, storms, sea level, and anthropogenic activities, especially in estuarine systems under the influence of coastal constructions. Hence, this study analyzes coastline changes along the severely affected Marismas Nacionales (MaNa) estuarine complex in Mexico over half a century, from 1970 to 2019. Our primary objective was to map shoreline variability before the construction of the Cuautla Canal in 1976 and to quantify erosion and accretion trends using a combination of aerial photographs and satellite data.

Materials and method

Study area

The MaNa complex lies on the Pacific coast of Mexico between the states of Sinaloa to the north and Nayarit to the south (Fig. 1). The coastline of this system presents a subtropical climate, with a mean annual temperature of

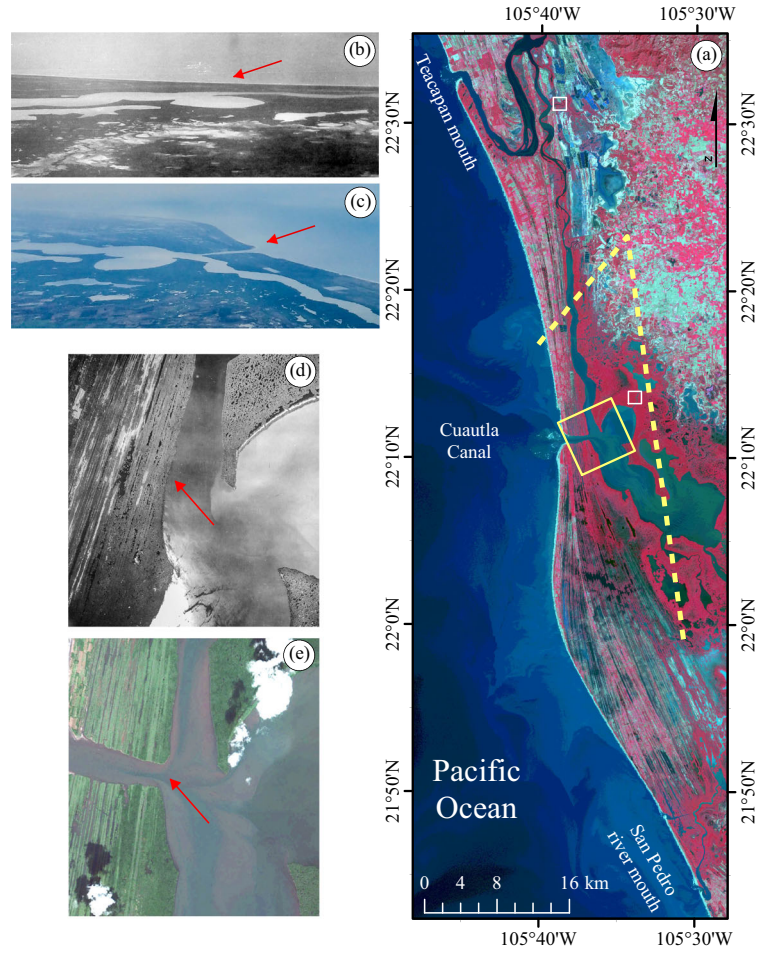

Fig. 1 **a** Location of the Marismas Nacionales coastline, Pacific coast of Mexico (Enhanced Near-infrared, Red, and Green of Sentinel-2 dated February 15, 2019). The two small yellow squares indicate the location of the Cañas River at the north, and the Acaponeta River at the south. The yellow dashed line represents the approximate field-of-view of both oblique aerial photographs: **b** taken in 1943 before the construction of the Cuautla Canal (red arrow) and **c** in 2018. The large yellow square marks the location of Cuautla Canal inlet: **d** vertical aerial photograph taken in 1960 and **e** the only available very-high spatial resolution Google Earth image unhampered by cloud cover (November 2009)

25 °C (INEGI 2016). Overall precipitation ranges from 850 mm at the northern edge in Teacapán, to approximately 1660 mm at the south section near the San Pedro River mouth. Indeed, maximum precipitation occurs during the tropical storms and hurricane season between the months of May and September, which causes a seasonally marked flooding pulse. Likewise, coastal waves show maximum energy during this season, presenting an overall northeastern direction. Coastal winds are predominant from the northwest during the winter months and from the west to the southwest during the summer months. The tidal amplitude presents a semidiurnal pattern with a mean height of 1.25 m along the coastline (Cruz-González 2012).

Twelve rivers have influenced the MaNa system (Blanco y Correa et al. 2011). Among such streams, freshwater from the San Pedro and Santiago rivers has had direct influence on the southern part of the coastline. Both rivers discharge directly into the Pacific Ocean, separated by 12 km of beach deposits. The more massive river of this area is the Santiago River, which has prograded towards the edge of the continental shelf with deltaic sediments for centuries (Curray et al. 1969). The Acaponeta and San Pedro rivers, located in the central part of the study site, present no infrastructure through their watershed. The remaining ten rivers show some water-controlled structure through their caudal. MaNa presents a unique geomorphologic feature that consists of a series of 280 parallel beach ridges located between the Cuautla Canal and the San Pedro River mouth. The ridges separate the mangrove forests within the coastal lagoon from the shoreline of the Pacific coast and are formed by coastal accretion processes due to constant transport of suspended sediments derived from the main rivers (i.e., Acaponeta, San Pedro, and Santiago) into the coastal plain (Curray et al. 1969).

The opening of the Cuautla Canal in 1976 severely impacted the entire MaNa system, causing drastic

hydrological changes throughout the lagoon complex that have adversely affected the mangrove forests due to changes in salinity levels (Serrano et al., 2019) and tidal regime (Kovacs et al. 2009). Specifically, Kovacs et al. (2001) used multi-temporal Landsat data and reported that an extensive area of mangrove forests has degraded in both the northern and southern sections of the Teacapán and Cuautla mouths. More recently, Kovacs et al. (2005) and Valderrama-Landeros et al. (2018) confirmed the aforementioned results using spaceborne images with higher spatial resolution.

Remote sensing data acquisition, coastal delimitation, and sea-surface elevation estimation

Individual aerial photographs were acquired from the Instituto Nacional de Estadística y Geografía (INEGI, Mexico) and the ICA Foundation. The available Landsat data were downloaded via http://earthexplorer.usgs.gov. The SPOT-5 data were obtained from the Secretaría de Marina Armada de México (SEMAR, Mexico) through the Estación de Recepción México de la Constelación SPOT (ERMEX). The Sentinel-2 data were downloaded via the European Space Agency (https://sentinel.esa.int/web/sentinel). The aerial photographs and satellite images were orthorectified and georeferenced separately based on a series of ground control points (e.g., roads, channels). The resulting scale and minimum mapping unit for all of the 10 remote sensing images were 1:50,000 and 1 ha, respectively. Finally, the mean sea level at the time of image acquisition was calculated given the possible influence of the tidal flooding amplitude on the coastline delimitation. The specific mean sea level (MSL) was determined using the lunar semi-diurnal M2 tidal amplitude harmonic from freely available software downloaded at the Centro de Investigación Científica y de Educación Superior de Ensenada (http://predmar.cicese.mx/programa/). The date and time of each satellite image were corrected using GMT − 7 from the closest tidal station (San Blas, Nayarit) located at the southern section of the MaNa system (Table 1).

The online base maps consist of national-level vector data within a frequently updated GIS platform, and include a series of layers of geomorphological, topographical, and hydrological frameworks (https://www.inegi.org.mx/app/mapas/). The series of analog aerial photographs were scanned and adjusted for scale, and their coastline was digitized using the commonly employed analog (visual) image processing method (Boak and Turner 2005). We used the near-infrared waveband (NIR) in order to separate coastal landforms from the sea in the remaining spaceborne images. Specifically, we selected the NIR waveband because it is well-known that this region of the electromagnetic spectrum enhances the interface between land and water due to the inherent optical properties of water (Jensen 2005; Valderrama-Landeros & Flores-de-Santiago et al., 2019). The digital shorelines from each remote sensing data source were separated and vectorized into a shapefile format in ArcMap v10.3. We identified the overall differences in the land cover features through the coastal region between the 1970 aerial photograph and the Sentinel-2 image of 2019, using the vector files. We specifically selected six representative classes for this study area: sand deposits, terrestrial vegetation, mangrove forest, agricultural fields, non-forested wetlands, and infrastructure. Monthly sea-surface circulation (direction and speed) and sea-surface elevation data (2013–2017) were obtained in NetCDF format from the Copernicus database (European Space Agency) via https://www.esa.int/Applications/Observing_the_Earth/Copernicus. Sea-surface circulation data were processed in the open-source software R using the netcdf4 function in order to obtain the u and v components. We plotted surface circulation vectors using the open-source software QuantumGIS. The sea-surface elevation (cm) maps were generated using a pixel-by-pixel mesh in QuantumGIS software.

Coastal analysis using the GIS-based DSAS method

The traditional software Digital Shoreline Analysis System (DSAS) automatically determines coastal change rates using several vectorized shorelines through a GIS-based routine (Thieler and Danforth 1994). DSAS v4.03.4730 is an extension tool of ArcGIS v10.3 software, which was developed jointly by the US Geological Survey (USGS) and the TPMC Environmental Services. The DSAS method automatically generates transect lines perpendicular to the coastal baseline and across the shoreline at specific intervals determined by the user. Actual rate-of-change variables are quantified using each coastline intersection among transects. In this study, we generated 955 transects at a 100-m spacing distance and at about 2 km perpendicular to the coastal baseline. It is beyond the scope of this article to

Table 1 Remote sensing data collected for the DSAS analysis. Estimated mean sea level (MSL) at the San Blas station (GMT − 7) based on software http://predmar.cicese.mx/programa/. RMSE (m) based on the geometric correction using ground control points

Data source	Date of acquisition (mm/dd/yyyy)	Time of acquisition (GMT)	Estimated MSL (m) at collection	Pixel spacing (m)	RMSE (m)
Air photo	ND/ND/1970	16:44	ND	4.5	< 1
Landsat-MSS	10/12/1980	16:50	+ 0.37	60	31.5
Landsat-TM	03/19/1986	16:44	− 0.19	30	4.6
Landsat-TM	04/15/1990	16:33	− 0.05	30	4.8
Landsat-TM	04/13/1995	16:59	− 0.02	30	4.9
Landsat-TM	04/26/2000	16:59	− 0.24	30	4.8
SPOT-5	12/01/2005	17:58	− 0.08	10	< 1
SPOT-5	03/26/2010	17:51	− 0.41	10	< 1
SPOT-5	02/28/2015	16:33	− 0.15	10	< 1
Sentinel-2	02/15/2019	17:34	− 0.31	10	< 1

explicitly review existing shoreline extraction methods, but several reviews on such approaches exist (e.g., Boak and Turner 2005; Gens 2010; Nel et al. 2014; Román-Rivera and Ellis 2019).

As a general rule, the shoreline movement difference concerning the baseline is considered a seaward shift (accretion) and a landward shift (erosion) at each transect, and the statistical values represent accretion (positive) and erosion (negative) trends. The DSAS provides five statistical operations in order to quantify shoreline variability, including end point rate (EPR), least median of squares (LMS), linear regression rate (LRR), net shoreline movement (NSM), and shoreline change envelop (SCE) (Thieler and Danforth 1994). Among these five available results, EPR calculates the rate of shoreline movement between two consecutive vectorized maps, and NSM is the average distance covered in the obtained images. The overall shoreline movement distance was represented for all of the available vectorized maps, and the coastal rates of erosion and accretion were quantified according to the coastal baseline location.

Results

Figure 2 depicts the overall accretion and erosion areas between 1970 and 2019. The total erosion area (red zone) is 50% larger than the accretion area (green zone) along the MaNa coastline. Specifically, the coastline located at the Cuautla Canal and in front of the beach ridges presents 805 ha of erosion, while the coastline next to the Teacapán mouth and the San Pedro River mouth shows 406 ha of accretion, with minimum variability along the remaining coastline. The highest land classification losses at the MaNa coastline were sand deposits (468 ha), followed by terrestrial vegetation (122 ha), mangrove forest (107 ha), agricultural fields (82 ha), non-forested wetlands (17 ha), and infrastructure (9 ha). Conversely, 356 ha from the accretion area were comprised of sand deposits, followed by non-forested wetlands (31 ha), terrestrial vegetation (10 ha), and mangrove forests (9 ha). The historical (2013 to 2017) monthly averaged sea surface circulation and sea-elevation model shows a littoral current (i.e., 10 km from the coast) with a predominant southern direction year-round (Fig. 3). Moreover, the sea surface height model depicts higher elevations during the summer months of July to August, corresponding to the typical spring tides of this region. Ocean circulation away from the coast (~ 20 km) shows a southern direction from February to April and from October to December. However, there is a reverse pattern during the hurricane season between May and September, with an overall northern direction.

Figure 4 depicts the EPR (m/year) interval (1970 to 2019). We separated the EPR diagram into northern and southern sections based on the position of the Cuautla Canal. Although both segments show similar pattern in general, a number of particular anthropogenic and natural events affected the accretion and erosion trends during specific periods. For instance, there was a higher accretion rate in the north (4.4 m/year) and lower one in the south (0.07 m/year) at the beginning of the historical

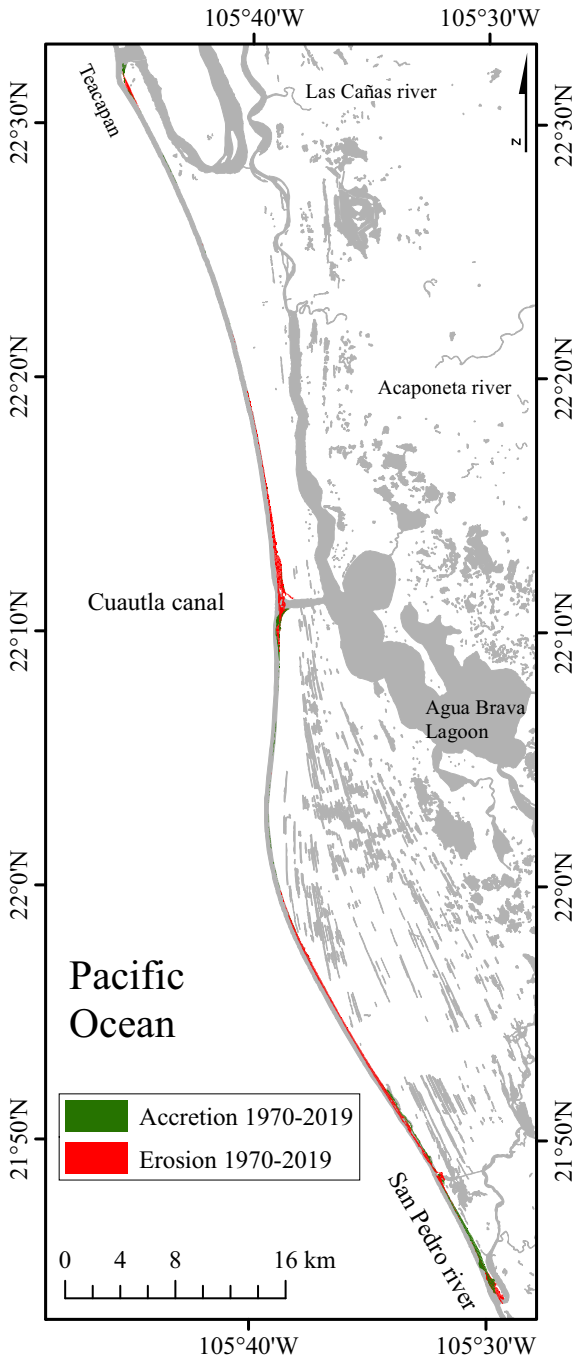

Fig. 2 Overall accretion and erosion areas throughout Marismas Nacionales coastline based on DSAS (1970–2019)

data (i.e., 1970–1980), even though two tropical storms (Eilee in 1970 and Priscilla in 1971) directly impacted the study site. There was an apparent erosion rate in the period from 1980 to 1986 after the Cuautla Canal opening in 1976 with − 8.7 m/year and − 4.1 m/years at the north and south locations, respectively. Tropical storms Otis in 1981 and Adolph in 1983, as well as category 4 hurricane Tico in 1983, impacted the north section of the Teacapán mouth and the southern section of the Caimanero lagoon (50 km north of the Teacapán mouth), respectively. Consequently, their natural effects, such as waves, storm surge, and winds, could have increased the erosion trend detected in the EPR diagram during this period.

The overall accretion rate from 1986 to 1990 was of 1.04 m/year and 2.03 m/year at the north and south sections, respectively, with no natural events along the coastline. This was also the case from 1990 to 1995, with 1.06 m/year and 3.4 m/year in the north and south sections, respectively. However, the increase in erosion from 1995 to 2000 at the north (− 2.7 m/year) and south (− 1.4 m/year) locations could be explained by the impact of category 1 hurricane Diana in 1990 and the hydroelectric Agua Milpa dam construction in 1993. It is thus believed that such events changed the overall coastline pattern. Moreover, hurricanes Rosa (category 2, 1994), Dolly (category 1, 1996), and Hernan (category 1, 1996) impacted the southern section of the study area during this period. The erosion rate was exacerbated during the next sequence of images between 2000 and 2005, due to the aforementioned causes and the addition of hurricane Kena (category 2, 2002), with − 9.1 m/year and − 9.9 m/year at the north and south sections, respectively. The absence of recorded tropical storms and hurricanes between 2005 and 2015 was reflected by the minimum variability, but the overall erosion rate was persistent at the north section, as was the accretion rate at the south. Finally, there was an erosion rate of − 0.16 m/year in the north and an accretion rate of 5.9 m/year in the south from 2015 to 2019, due to the massive hurricane Willa (category 5, 2018) that directly impacted the Teacapán mouth.

Figure 5 shows the specific accretion and erosion NSM distance (m) of the first 10 km of coastline from the Cuautla Canal mouth. We decide to separate both NSM diagrams because the most dynamic region was the Cuautla Canal mouth (Fig. 2), and thus detailed temporal NSM results were enhanced. In general, there was an overall accretion distance of ~ 250 m on both sides between 1970 and 1980. On the other hand, the Cuautla Canal mouth presented an overall erosion of ~ 100 m during the following period between 1980 and 1986. Erosion and accretion distances were minimum (< 25 m) from 1986 to 1990, as opposed to an overall

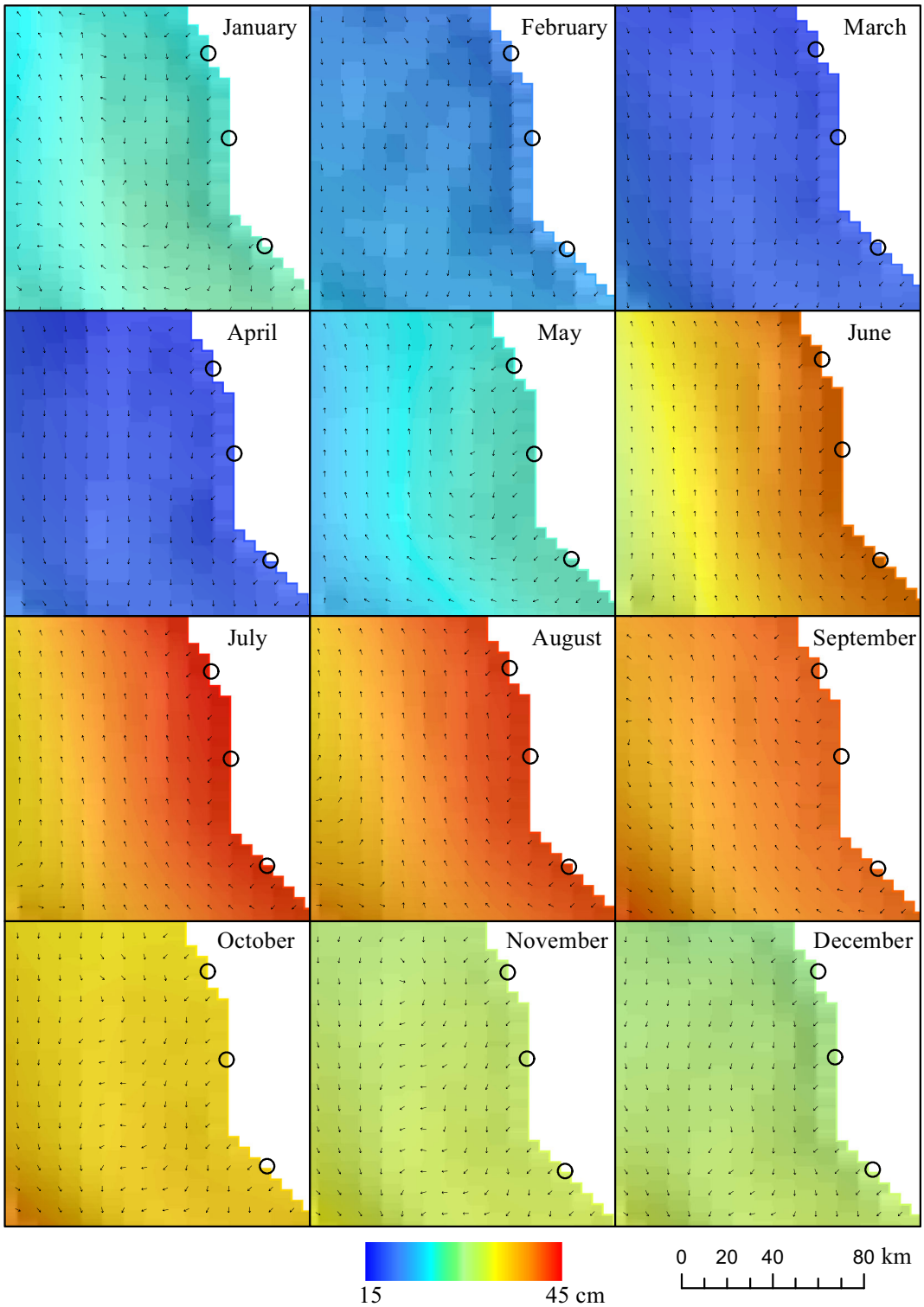

Fig. 3 Historical (2013–2017) averaged surface circulation current vectors and sea-surface elevation data. From north to south, hollow circles represent the Teacapán mouth, the Cuautla Canal, and the San Pedro River mouth locations

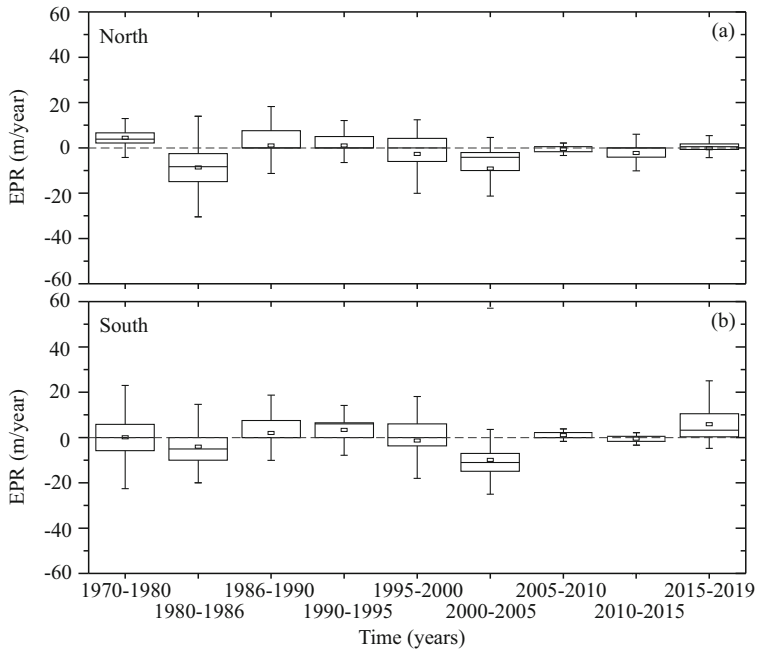

Fig. 4 End point rate (m/year) along the Marismas Nacionales shoreline. The **a** north and **b** south sections were divided according to the Cuautla Canal mouth for easier representation. Positive values represent accretion while negative values indicate erosion

higher erosion distance of ~ 450 m from 1990 to 1995, although only at the southern section of the Cuautla Canal. Higher erosion (~ 750 m south and ~ 350 m north) was presented during 1995 to 2000, but only along the first 2 km from the mouth. There was a higher erosion distance in the north (~ 550 m) from 2000 to 2005. However, considerable accretion (~ 250 m) along the first km at the north and minor accretion in the south section were observed between 2005 and 2010. A relatively stable condition was found during 2010 to 2015 with minimum accretion of less than 25 m, whereas the southern section of the study site presented considerable accretion (~ 300 m) from 2015 to 2019.

Discussion

Although the MaNa coastal system is considered the largest wetland complex of the western Pacific Ocean, our results indicate that this environment strongly depends on the sediment input from rivers and on sediment transport from the littoral current (Blanco y Correa et al. 2011). The strong correlation between beach deposits and river-supplied sediments, as well as shoreline degradation due to coastal infrastructure, is well-known (Kim et al. 2017; Williams et al. 2018). Therefore, hydroelectric constructions could hinder the available sediment supply into coastal systems, and coastal infrastructure could alter the hydrological patterns within wetland systems (Moussaid et al. 2015). Our results indicate that the shoreline position over a mid-centennial period (49 years) was subject to either accretion or erosion trends, contingent on the influence of the available river discharge and the opening of the Cuautla Canal in 1976. Specifically, 806 ha of the coastline had been eroded at the Cuautla Canal inlet and in front of the beach ridges (i.e., former depositional sites), in contrast to the 406 ha of beach deposits we detected along the San Pedro River mouth and the Teacapán mouth with the latter being influenced by the unobstructed Acaponeta River (Ezcurra et al. 2019).

The coastal plain of MaNa can be considered a delta influenced by 12 rivers that have combined into a primary coastal lagoon with several beach ridges. According to Curray (1969), this coastal system represents an example of the turning point from shoreline transgression to regression across the continental shelf due to the eustatic sea-level rise (7000 years before the present). Hence, recent erosion at the beach ridges location could represent a realignment of the coastline in response to changes in oceanographic conditions and the sediment supply rate. However, the erosion pattern found in our study could be a response to the relatively recent lack of sediment supply (Ezcurra et al. 2019; Valderrama-Landeros and Flores-de-Santiago 2019) as well as to the internal hydrodynamic changes resulting from the opening of the Cuautla Canal (Serrano et al., 2019).

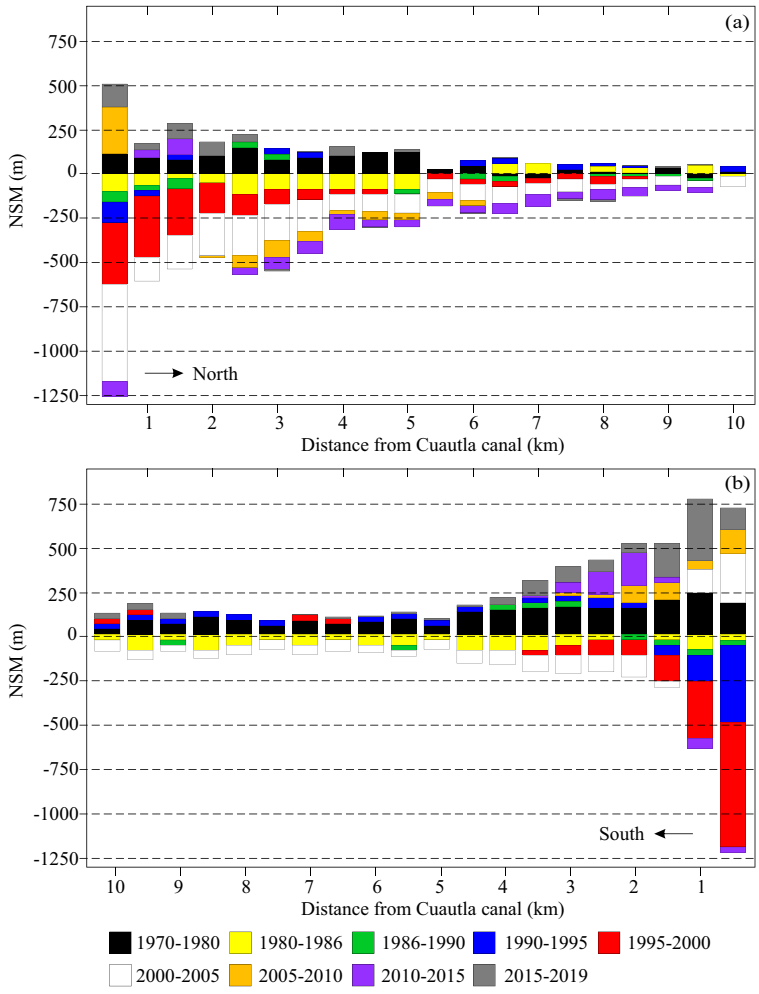

Fig. 5 Net shoreline movement (m) along the first 10 km of coastline from the Cuautla Canal mouth. Horizontal black arrows indicate shoreline direction from the Cuautla Canal mouth at the north (**a**) and south (**b**)

Regarding the mangrove forest extension at the coastline of the MaNa system, there are three dominant mangrove species: the black mangrove (*Avicennia germinans*), the white mangrove (*Laguncularia racemosa*), and the red mangrove (*Rhizophora mangle*). Our results indicate that 107 ha of mangrove forests have been loss, with only 9 ha of mangrove expansion. The mangroves of this coastal system have experienced considerable degradation due to the adverse hydrologic changes (e.g., hypersalinity and tidal regime) that followed the opening of the Cuautla Canal in 1976 (Flores-Verdugo et al. 1990; Kovacs et al. 2005; Serrano et al., 2019). For instance, Rollet (1974) had reported a lack of anthropogenic disturbances or mangrove degradation before the Cuautla Canal opening and had observed that the large mangrove trees within the MaNa system were due to low salinity concentration. However, it was not until a decade later that Flores-Verdugo et al. (1990) would note a major degradation of the mangrove forests of the Teacapán-Agua Brava lagoon section, thereby proposing that the Cuautla Canal has developed a negative effect on the mangrove forests by altering the natural hydrological pattern, which led to increased water salinity.

Regarding shoreline variability, coastal erosion in this study site has been assessed along the main river mouths by comparing the influence of sediment trapped in hydroelectric power dams (e.g., Ezcurra et al. 2019; Valderrama-Landeros and Flores-de-Santiago 2019). According to the EPR diagram, it is clear that the opening of the Cuautla Canal caused an overall erosion trend along with the MaNa system during the 1980 to 1986 period. Moreover, hydrodynamic modeling of the MaNa system indicated that the opening of the Cuautla Canal created strong and permanent tidal friction through the inlet, causing major coastal erosion (Serrano et al. 2019). Indeed, the same situation was seen after the construction of the Agua Milpa

dam in 1993 with an overall erosion trend from 1995 to 2000, and this erosion was exacerbated by the impact of category 4 hurricane Kena in 2002. Contrary to the aforementioned results, it appears that the MaNa coastline had maintained a degree of stability from 2005 to 2019, and that even some accretion events had been registered at the southern section. However, natural events such as massive category 5 hurricane Willa affected the overall shoreline dynamic, as evidenced by the differences in the EPR diagram between the northern and southern sections. Even though it has been reported that the Cuautla Canal has changed the hydrodynamic patterns throughout the MaNa wetland (Serrano et al., 2019), the direct erosion trend along the Cuautla Canal could be considered very site-specific based on the NSM diagram. Indeed, it appears that the Cuautla Canal has become relatively more stable, and this information was confirmed with the recruitment of mangrove trees along the main inlet, whose overall erosion pattern decreased from 1995 to 2005.

Changes in natural conditions throughout the MaNa system, including freshwater input and hydrological connectivity, have modified its ecological structure, such as mayor wetland and coastal losses due to salinity variability and sediment transport. These adverse anthropogenic effects may propagate throughout adjacent coastal systems (Mahoney and Bishop 2017). The situation could be additionally exacerbated by poor land-use planning and climate change, such as an increase in sea level that could result in coastal erosion further landward and at higher tidal elevations, extending the magnitude of flooding events (Rogers and Woodroffe 2016). Indeed, coastal planners and policymakers need an accurate historical indicator of the vulnerability of coastal systems to erosion and inundation processes, and we should leverage this information to contribute to dynamic coastal research. In this sense, the method utilized in this study was found to be a practical approach for assessing changes in shoreline position through time. Specifically, the detection of shoreline evolution was feasible by using a combination of aerial photographs, moderate spatial resolution Landsat, SPOT, and Sentinel data, and GIS-based analysis. However, some limitations need to be considered, such as the different spatial resolutions, satellite data cost, and sea-surface elevation due to tidal dynamics.

Regarding spatial resolution, it is clear that aerial photographs and coarse spatial resolution Landsat data have been the only available historical remote sensing data (Wulder et al. 2016) since the first Landsat satellite was launched in the early 1970s (Boak and Turner 2005). By contrast, very-high spatial resolution data such as WorldView, IKONOS, and QuickBird images are expensive, and continuous image availability is minimal. Nevertheless, it has become apparent, mainly through the considerable shoreline loss at the Cuautla Canal mouth (1250 m), that coastline delineation was unhampered by relatively coarse spatial resolution satellite data in the study site. Moreover, our coastal trends are similar to those reported by Cruz-González (2012) and Ezcurra et al. (2019).

The other major limitation that could affect our results consists of the tidal variability among the remote sensing data sources. In this regard, Gens (2010) suggested that tidal amplitude is more likely to affect very-high spatial resolution satellite data than coarser spatial resolution images. It is difficult, if not nearly impossible, to acquire spaceborne images during the same tidal conditions because of different satellite orbital paths; however, we believe that our results were not hindered by the different tidal amplitudes (Table 1), because the MaNa coastline has been classified as a continental collision coast (Inman and Nordstrom 1971) with a typical abrupt foreshore height of ~ 1 m, according to the beach profiles by Cruz-González (2012). Consequently, the combination of a narrow continental shelf and low semi-diurnal tidal amplitude could result in minimal influence by tidal differences using coarse spatial resolution spaceborne data.

It has been suggested that the geomorphological properties of this coastal system are enhanced in relation to its proximity to the river mouths (Cruz- González 2012). For instance, the beach ridge zone has been characterized as a constant accretion region due to the presence of the Acaponeta, Bejuco, Rosa Morada, and San Pedro rivers (Evans 1979). However, erosion processes are continuously detected in the southern section of these beach ridges southwards to the San Pedro River mouth. On the other hand, the coastal area located from the Cuautla Canal to the northern section of the beach ridges presents a relatively stable coast. Since this area was affected by the opening of the Cuautla Canal, we believe that the suspended sediments transported by the Acaponeta River are carried into the ocean throughout the Cuautla Canal and then distributed to the southern section of the coastline via the littoral current (Fig. 3). However, these suspended sediments may not always reach the beach ridge shoreline location, and thus erosion processes are more common farther away from the Cuautla Canal's influence. In fact, De-la-Lanza-Espino

et al. (2012) indicated that the annual Acaponeta River volume (981 hm^3) is the only freshwater and sediment source of the MaNa system.

Conclusions

The results of this study emphasize the feasibility of synergy among historical remote sensing data with medium to high spatial resolutions and automatic GIS calculation process (DSAS) in providing reliable information on coastal geomorphological dynamics for conservational purposes. Understanding historical shoreline trends in a complex system, such as MaNa contributes to the comprehension of major implications for the effective management of this crucial coastal environment. Although our results are based on remote sensing data, they are expected to provide more insight into future coastal management decisions, such as major coastal infrastructure programs in subtropical estuarine areas. Unfortunately, the absence of comprehensive empirical baseline studies based on biodiversity data, or data comprising additional ecological parameters, such as wetland ecosystem function and services in this region, impedes the quantification of the absolute magnitude of ecological impacts, such as fisheries and carbon burial, due to coastal structures and upstream damns.

The overall erosion (805 ha) and accretion (406 ha) areas were mapped and detailed using remote sensing data and automatic GIS analysis (i.e., DSAS) during the 49 years (1970–2019). Our study detected temporal coastal geomorphological trends according to major infrastructure projects, such as the Cuautla Canal opening, the construction of the Agua Milpa dam, and even natural phenomena, such as tropical storms and hurricanes along the MaNa coastal region. Also, major erosion processes were detected in front of the beach ridge section that should otherwise be an accretional coastal zone due to the influence of several rivers, although most of this suspended sediment is directly transported into the ocean through the inlet or abducted by the dams.

Acknowledgments We express our gratitude to the Instituto Nacional de Estadística y Geografía (INEGI) and the ICA Foundation for providing the available air photographs. Guillermina Fehér edited the English text.

Funding information FFdS acknowledges financial support for this research through a grant provided by the Instituto de Ciencias del Mar y Limnología (ICML, UNAM, Mexico #622)

References

Ahmed, N., & Glaser, M. (2016). Coastal aquaculture, mangrove deforestation and blue carbon emissions: is REDD+ a solution? *Marine Pollution, 66*, 58–66.

Bishop, M. J., Mayer-Pinto, M., Airoldi, L., Firth, L. B., Morris, R. L., Loke, L. H. L., et al. (2017). Effects of ocean sprawl on ecological connectivity: impacts and solutions. *Journal of Experimental Marine Biology and Ecology, 492*, 7–30.

Blanco y Correa, M., Flores-Verdugo, F., Ortiz-Pérez, M. A., de la Lanza-Espino, G., López-Portillo, J., & Valdez-Hernández, I. (2011). *Diagnostico funcional de Marismas Nacionales*. Nayarit, Mexico: Informe de los convenios de coordinación entre la Universidad Autónoma de Nayarit y la Comisión Nacional Forestal con el patrocinio del Gobierno del Reino Unido.

Boak, E. H., & Turner, I. L. (2005). Shoreline definition and detection: a review. *Journal of Coastal Research, 21*(4), 688–703.

Cruz-González, M. (2012). *Variaciones estacionales en la línea de costa entre el Canal de Cuautla y el Estero de San Cristóbal, Nayarit*. Dissertation: Universidad Nacional Autónoma de México.

Curray, J. R., Emmel, P. J., & Crampton, P. J. S. (1969). Holocene history of a strand plain, lagoonal coast, Nayarit. *Mexico. Simposio Internacional de Lagunas Costeras*, 63–100.

De-la-Lanza-Espino, G., Carbajal-Pérez, J. L., Salinas-Rodríguez, S. A., & Barrios-Ordóñez, J. E. (2012). Medición del caudal ecológico del río Acaponeta, Nayari, comparando distintos intervalos de tiempo. *Investigaciones Geográficas, Boletín del Instituto de Geografía, UNAM, 78*, 62–74.

Evans, G. (1979). Quaternary transgressions and regressions. *Journal of the Geological Society of London, 136*, 125–132.

Ezcurra, E., Barrios, E., Ezcurra, P., Ezcurra, A., Vanderplank, S., Vidal, O., et al. (2019). A natural experiment reveals the impact of hydroelectric dams on the estuaries of tropical rivers. *Science Advancements*, 5, eaau9875.

Flores-Verdugo, F., González-Farías, F., Ramírez-Flores, O., Amezcua-Linares, F., Yáñez-Arancibia, A., Álvarez-Rubio, M., et al. (1990). Mangrove ecology, aquatic primary productivity, and fish community dynamics in the Teacapán-Agua Brava lagoon-estuarine system (Mexican Pacific). *Estuaries, 13*(2), 219–230.

Gens, R. (2010). Remote sensing of coastlines: detection, extraction and monitoring. *International Journal of Remote Sensing, 31*(7), 1819–1836.

Harik, G., Alameddine, I., Maroun, R., Rachid, G., Bruschi, D., Astiaso-Garcia, D., et al. (2017). Implications of adopting a biodiversity-based vulnerability index versus a shoreline environmental sensitivity index on management and policy planning along coastal areas. *Journal of Environmental Management, 187*, 187–200.

INEGI. (2016). *Anuario estadístico y geográfico de Nayarit 2016*. Ciudad de México, Mexico: Instituto Nacional de Estadística y Geografía.

Inman, D. L., & Norstrom, C. E. (1971). On the tectonic and morphologic classification of coasts. *Journal of Geology, 79*(1), 1–21.

Jensen, J. R. (2005). *Introductory digital image processing: a remote sensing perspective*. Upper Saddle River, NJ: Prentice Hall.

Kim, J., Choi, J., Choi, C., & Hwang, C. (2017). Forecasting the potential effects of climatic and land-use changes on shoreline variation in relation to watershed sediment supply and transport. *Journal of Coastal Research, 33*(4), 874–888.

Kovacs, J. M., Wang, J., & Blanco-Correa, M. (2001). Mapping disturbances in a mangrove forest using multi-date Landsat TM imagery. *Environmental Management, 27*(5), 763–776.

Kovacs, J. M., Wang, J., & Flores-Verdugo, F. (2005). Mapping mangrove leaf area index at the species level using IKONOS and LAI-2000 sensors for the Agua Brava Lagoon, Mexican Pacific. *Estuarine, Coastal and Shelf Science, 62*, 377–384.

Kovacs, J. M., King, J. M. L., Flores-de-Santiago, F., & Flores-Verdugo, F. (2009). Evaluating the condition of a mangrove forest of the Mexican Pacific based on an estimated leaf area index mapping approach. *Environmental, Monitoring and Assessment, 157*, 137–149.

Leuven, J. R. F. W., Kleinhans, M. G., Weisscher, S. A. H., & van der Vegt, M. (2016). Tidal sand bar dimensions and shapes in estuaries. *Earth-Science Reviews, 161*, 204–223.

Maanan, M., Maanan, M., Rueff, H., Adouk, N., Zourarah, B., & Rhinane, H. (2018). Assess the human and environmental vulnerability for coastal hazard by using a multi-criteria decision analysis. *Human and Ecological Risk Assessment, 24*(6), 1642–1658.

Mahoney, P. C., & Bishop, M. J. (2017). Assessing risk of estuarine ecosystem collapse. *Ocean and Coastal Management, 140*, 46–58.

McLeman, R. (2018). Migration and displacement risks due to mean sea-level rise. *Bulletin of the Atomic Scientists, 74*(3), 148–154.

Moussaid, J., Fora, A. A., Zourarah, B., Maanan, M., & Maanan, M. (2015). Using automatic computation to analyze the rate f shoreline change on the Kenitra coast, Morocco. *Ocean Engineering, 102*, 71–77.

Nassar, K., Fath, H., Mahmod, W. E., Masria, A., Nadaoka, K., & Negm, A. (2018). Automatic detection of shoreline change: case of North Sinai coast, Egypt. *Journal of Coastal Conservation, 22*(6), 1057–1083.

Nel, R., Campbell, E. E., Harris, L., Hauser, L., Schoeman, D. S., McLachlan, A., et al. (2014). The status of sandy beach science: past trends, progress, and possible futures. *Estuarine, Coastal and Shelf Science, 150*, 1–10.

Ouyang, X., Lee, S. Y., & Connolly, R. M. (2017). The role of root decomposition in global mangrove and saltmarsh carbon budgets. *Earth-Science Reviews, 166*, 53–63.

Perkins, M. J., Ng, T. P. T., Dudgeon, D., Bonebrake, T. C., & Leung, K. M. Y. (2015). Conserving intertidal habitats: what is the potential of ecological engineering to mitigate impacts of coastal structures? *Estuarine, Coastal and Shelf Science, 167*, 504–515.

Powell, E. J., Tyrrell, M. C., Milliken, A., Tirpak, J. M., & Staudinger, M. D. (2019). A review of coastal management approaches to support the integration of ecological and human community planning for climate change. *Journal of Coastal Conservation, 23*(1), 1–17.

Rogers, K., Kelleway, J. J., Saintilan, N., Megonigal, J. P., Adams, J. B., Holmquist, J. R., Lu, M., Schile-Beers, L., Zawadzki, A., Mazumder, D., & Woodroffe, C. D. (2019). Wetland carbon storage controlled by millennial-scale variation in relative sea-level rise. *Nature, 567*, 91–95.

Rogers, K., & Woodroffe, C. D. (2016). Geomorphology as an indicator of the biophysical vulnerability of estuaries to coastal and flood hazards in a changing climate. *Journal of Coastal Conservation, 20*, 127–144.

Rollet, B. (1974). Introduction a l'étude des mangroves du Mexique. *Bois et Forets des Tropiques, 156*, 3–26.

Román-Rivera, M. A., & Ellis, J. T. (2019). A synthetic review of remote sensing applications to detect nearshore bars. *Marine Geology, 408*, 144–153.

Serrano, D., Flores-Verdugo, F., Ramírez-Félix, E., Kovacs, J. M., & Flores-de-Santiago, F. (2019). Modeling tidal hydrodynamic changes induced by the opening of an artificial inlet within a subtropical mangrove dominated estuary. *Wetlands Ecology, and Management.*, 1–16. https://doi.org/10.1007/s11273-019-09697-w.

Thieler, E. R., & Danforth, W. W. (1994). Historical shoreline mapping (II): application of the digital shoreline mapping and analysis systems (DSMS/DSAS) to shoreline change mapping in Puerto Rico. *Journal of Coastal Research, 10*(3), 600–620.

Valderrama-Landeros, L., Flores-de-Santiago, F., Kovacs, J. M., & Flores-Verdugo, F. (2018). An assessment of commonly employed satellite-based remote sensors for mapping mangrove species in Mexico using an NDVI-based classification scheme. *Environmental, Monitoring and Assessment, 190*, 23.

Valderrama-Landeros, L., & Flores-de-Santiago, F. (2019). Assessing coastal erosion and accretion trends along two contrasting subtropical rivers based on remote sensing data. *Ocean and Coastal Management, 169*, 58–67.

Williams, A. T., Rangel-Buitrago, N., Pranzini, E., & Anfuso, G. (2018). The management of coastal erosion. *Ocean and Coastal Management, 156*, 4–20.

Wulder, M. A., White, J. C., Loveland, T. R., Woodcock, C. E., Belward, A. S., Cohen, W. B., et al. (2016). The global Landsat archive: status, consolidation, and direction. *Remote Sensing of the Environment, 185*, 271–283.